



1 **Inter-annual variation of lake ice composition in European Arctic: observations based on high-**
2 **resolution thermistor strings**

3

4 Bin Cheng^{1*}, Yubing Cheng^{2,3,1*}, Timo Vihma¹, Anna Kontu¹, Fei Zheng², Juha Lemmetyinen^{1,5},
5 Yubao Qiu^{4,5} and Jouni Pulliainen¹

6 ¹ Finnish Meteorological Institute (FMI), Finland

7 ² Institute of Atmospheric Physics, Chinese Academy of Sciences, Beijing, China

8 ³ University of Chinese Academy of Sciences, Beijing, China

9 ⁴ Aerospace information Research Institute (AIR), Chinese Academy of Science, Beijing China

10 ⁵ FMI-AIR, Joint Research Center for Arctic Observations, Sodankylä, Finland.

11 *corresponding authors:

12 Bin Cheng (bin.cheng@fmi.fi)

13 Yubing Cheng (chengyubing@mail.iap.ac.cn)

14

15 Abstract

16 Climate change and global warming strongly impact the cryosphere. The rise of air temperature and
17 change of precipitation patterns lead to dramatic responses of snow and ice heat and mass balance.

18 Sustainable field observations on lake air-snow-ice-water temperature regime have been carried out
19 in Lake Orajärvi in the vicinity of the Finnish Space Centre, a Flagship Supersite in Sodankylä in
20 Finnish Lapland since 2009. A thermistor string-based snow and ice mass balance buoy called “Snow
21 and ice mass balance apparatus (SIMBA)” was deployed in the lake at the beginning of each ice
22 season. In this paper, we describe snow and ice temperature regimes, snow depth, ice thickness, and
23 ice compositions retrieved from SIMBA observations as well as meteorological variables based on
24 high-quality observations at the Finnish Space Centre. Ice thickness in Lake Orajärvi showed an
25 increasing trend. During the decade of data collection: 1) The November-May mean air temperature
26 had an increasing trend of 0.16° C/year, and the interannual variations were highly correlated ($r =$
27 0.93) with the total seasonal accumulated precipitation; 2) The maximum granular ice thickness



28 ranged from 15 to 80% of the maximum total ice thickness; 3) The snow depth on lake ice was not
29 correlated ($r = 0.21$) with the total precipitation. The data set can be applied to investigate the lake ice
30 surface heat balance and the role of snow on lake ice mass balance, and to improve the
31 parameterization of snow to ice transformation in snow/ice models. The data are archived at
32 <https://zenodo.org/record/4559368#.YIKOOpAzZPZ> (Cheng et al., 2021)

33

34 **1. Introduction**

35

36 The rapid climate warming in the Arctic (Box et al., 2019; Przybylak and Wyszyński, 2020) has also
37 affected lakes, in particular lake surface temperatures and lake ice phenology (Woolway, et al., 2019).
38 In the Northern Hemisphere, the lake ice season has become shorter and lake ice has become thinner,
39 and these trends are projected to continue throughout the 21st century (Sharma, et al., 2019). Lakes
40 are important in the Earth system, as they can adjust local climate (Brown and Duguay, 2010), and
41 affect the environment through interactions among physical, hydrological, biological, and chemical
42 processes (Leppäranta, 2010).

43 Observations on snow depth and lake ice thickness are needed for (a) monitoring of climate variability
44 and trends (Filazzola et al., 2020), (b) practical applications, such as use of lake ice for winter fishing,
45 transport, and recreational activities (Leppäranta, 2015), and (c) to provide initial conditions for
46 operational forecasting (Anderson et al., 2018). Snow depth and lake ice thickness can be measured
47 manually. For example, in Finland, lake ice thickness is measured via manual drilling in a single
48 location in 45 lakes with ten-day intervals throughout the ice season. However, this requires a lot of
49 manpower, and accordingly does not allow collection of time series with a better spatial and temporal
50 resolution. During recent decades, the number manual observations has strongly declined in many
51 countries (Duguay et al., 2006). Satellite remote sensing yields information on lake ice cover (Wu et
52 al., 2021) and snow/ice surface temperature (Cheng et al., 2014) with a sufficiently high spatial and
53 temporal resolution. Kang et al., (2014) introduced a method to derive lake ice thickness from coarse
54 resolution (~ 10 km) passive microwave data over large lakes in Canada. However, the transferability
55 of the method to sub-pixel scale lakes has not been investigated. SAR polarimetry has shown some
56 promise in retrieving ice depth over rivers (Mermoz et al., 2013); as fully polarimetric data is not to



57 date widely available from existing SAR sensors extensive testing and application of the method for
58 lakes is currently lacking.

59 The SIMBA data set is potentially highly relevant for the development of land applications for
60 planned and existing passive microwave satellite sensors, such as the Copernicus Imaging Microwave
61 Radiometer (CIMR), new Metop multichannel radiometer sensors of EUMETSAT, ESA SMOS,
62 NASA SMAP and Chinese sensors. Due to the inherent coarse resolution of these sensors (tens of
63 kilometers), a key issue is to acquire combined simultaneous data representing various processes in
64 lakes, in addition to surrounding land areas. As such, the SIMBA forms an integral part of the FMI
65 sensor network in Sodankylä.

66 Thermistor sting-based snow and ice mass balance apparatus (SIMBA) have been applied for more
67 than a decade to measure snow depth, ice thickness and temperature profile from air through snow
68 and ice to water (Jackson et al., 2013). Most of SIMBA have so far been deployed in Polar sea ice
69 (Lei et al., 2018), but also lake ice has been studied (Cheng et al., 2014; Wei et al., 2016). In this
70 paper we describe SIMBA observations from an ongoing program that started in Lake Orajärvi in
71 northern Finland in 2009. Supporting meteorological observations from Finnish Meteorological
72 Institute Arctic Research Centre (FMI-ARC) are also presented. The objectives of the SIMBA
73 program were

- 74 - to evaluate the cost-effectiveness of SIMBA buoys in a remote lake environment
- 75 - to monitor climate variability and change as reflected in snow depth as well as lake ice
76 thickness and composition
- 77 - to investigate (a) atmospheric forcing on lake ice growth and melt, (b) the role of snow on
78 lake ice mass balance via formation of superimposed ice due to refreezing of melt water
79 and rain and formation of snow ice due to flooding under a heavy snow load, and (c) the
80 role of granular ice in lake ice phenology
- 81 - to develop better parameterizations of snow-to-ice transformation in numerical snow/ice
82 models.

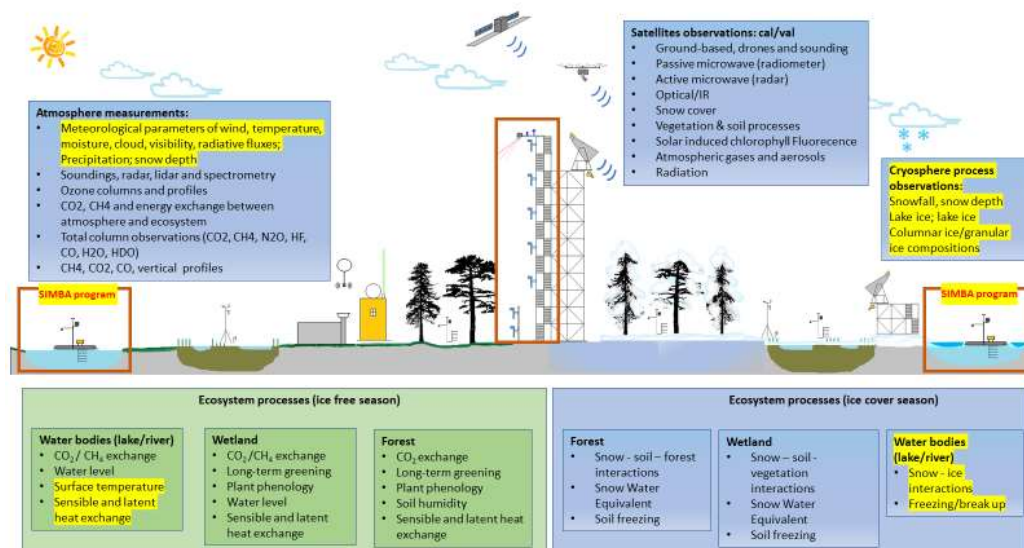
84 **2 Observation**

85 **2.1 Sodankylä supersite**

86 The SIMBA program at Lake Orajärvi is a component of the FMI Sodankylä supersite. The Finnish



87 Meteorological Institute's Arctic Space Centre (FMI-ARC) in Sodankylä (67.367 °N, 26.629 °E),
88 Finland, is a super-observation site where various Earth observations (upper-air chemistry and
89 physics, atmospheric column measurements, snow and soil hydrology, biosphere-atmosphere
90 interaction) and ground truth measurements for satellite calibration-validation are carried out
91 continuously (Fig.1). The site is equipped with comprehensive in situ and remote sensing
92 instrumentation placed in the forests, wetlands and freshwater bodies, which are the main landcover
93 types in the area. In this paper we focus on the cryospheric *in situ* observations of snow cover and
94 lake ice as well as meteorological parameters.



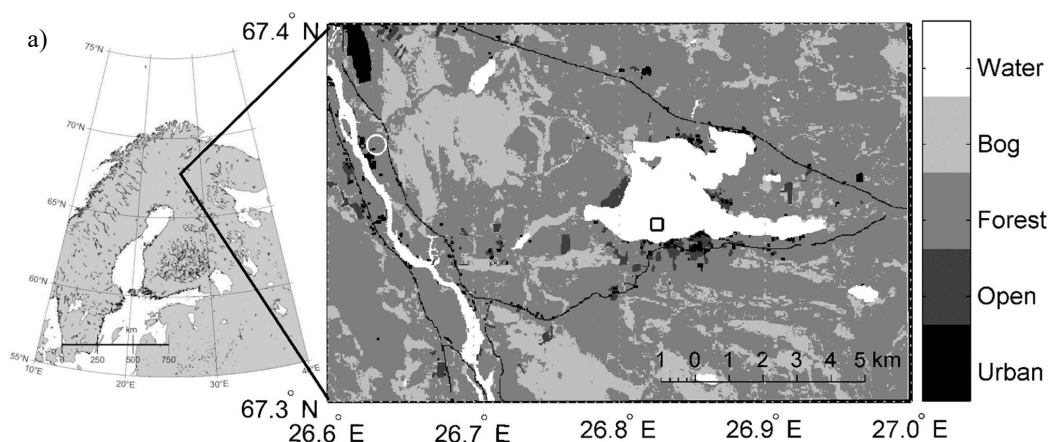
95
96 Figure 1. Schematic diagram of the FMI-ARC supersite observational systems at Sodankylä. The
97 original diagram is at <https://litdb.fmi.fi/>. The frames in red and text with yellow background
98 describes the measurements addressed in this paper.

99
100 The sub-Arctic climate and the geographic location between continental and marine climate zones
101 result in a high inter-annual, seasonal and synoptic-scale variation in local weather conditions,
102 enabling development of very different kinds of snowpack structures on land (Tikkanen, 2005) and
103 snow/ice composition on lakes (Cheng et al., 2014). Lake Orajärvi is a boreal medium-sized lake
104 located in Sodankylä municipality in the in the eastern Lapland. The lake has a surface area of about
105 11 km² with an average depth of 4.4 m and a maximum depth of 11 m close to the southern shore of



106 the lake (Fig. 2a). The estimated water volume in the lake is 0.0485 km^3 , and the shore length is 28
107 km. The lake surface elevation is 182 m above sea level. The ice season typically starts in November
108 and lasts until May. The first snowfall typically occurs in late October, but the snow may melt during
109 warmer autumn days. The seasonally permanent winter snow accumulation usually starts between
110 mid-November and early-December. Snow is present on the lake ice surface every winter season.

111



112



113

114

115 Figure 2. a) The location of Lak Orajärvi in Finnish Lapland and a map of lake Orajärvi and local
116 catchment, where the open black square marks the SIMBA site and white circle is the Finnish Space



117 Centre. b) Snapshots of SIMBA deployment in Lake Orajärvi and a weather station at FMI-ARC
 118 main camp. A raft was anchored in the lake in October 2019 aiming to extend the lake observations
 119 beyond the ice season.

120

121 2.2 SIMBA

122 2.2.1 SIMBA program

123 SIMBA buoys have been deployed in Lake Orajärvi since 2009. The 2009 deployment was probably
 124 the internationally first SIMBA application for a lake study. In each winter when ice was formed in
 125 Lake Orajärvi, one SIMBA was deployed around mid-December at the same site, 67.35° N, 26.83° E,
 126 some 500 m from the shoreline. At the time of deployment, the snow depth, lake ice thickness and
 127 ice freeboard were measured. A supporting frame made of fiberglass was constructed on lake ice, and
 128 the SIMBA main control Peli case was placed on top of it (Fig. 2b). A separate wooden pole with
 129 scale was standing vertically to hold the thermistor string. An ice borehole was drilled through the ice
 130 layer, and the thermistor string was placed in it. The scene was left as it is, and then the thermistor
 131 string was frozen with surrounding water in the borehole. The SIMBA operated in the lake over the
 132 winter and most of the spring melting season. The recovery of SIMBA took place usually in late April
 133 but in some years as late as mid-May. Snow and ice conditions around the deployment site were
 134 documented and measured before dismantling the SIMBA camp. The documentation on SIMBA
 135 deployment and recovery is provided along with the SIMBA data as online files (see data availability).
 136 Table 1 summarizes the SIMBA deployment and recovery status.

137

138 Table 1. SIMBA deployment and recovery days and simultaneous manually observed snow depth (h_s),
 139 total ice thickness (H_i), and ice freeboard (H_{fb} , defined as negative if the lake water level was above
 140 the snow/ice interface) The seasonal mean values were derived from SIMBA-ET and SIMBA-HT
 141 observations. H_{gi} is the granular ice and H_{ci} is the congelation ice thickness.

Season	Deployment				Recovery					Seasonal mean \pm STD				
	Date	h_s	H_i	H_{fb}	Date	h_s	H_{ci}	H_i	H_{fb}	H_i	h_s	H_{fb}	H_{gi}	H_{ci}
	DD/MM/YY	(cm)			DD/MM/YY	(cm)								
2009/2010	16/12/09	5	27	0	07/04/10	31	54	64	5	NA				
2010/2011	SIMBA was not deployed; only manual observations every second week were available.													



2011/2012	19/12/2011	16	14	-4	12/04/2012	24	22	55	-3	38±16	22±6	5±2	15±10	23±7
2012/2013	12/12/2012	18	33	+1	25/04/2013	0	39	59	6	57±7	26±7	-5±3	4±4	53±4
2013/2014	12/12/2013	14	27	+1	30/04/2014	20	35	35	-3	49±7	17±4	-3±2	10±2	40±6
2014/2015	14/12/2014	19	30	-2.5	23/04/2015	2	35	69	4	54±11	24±7	-4±3	16±8	38±4
2015/2016	18/12/2015	18	27	-1	22/04/2016	5	30	71	6	60±16	19±7	-2±3	12±9	48±9
2016/2017	16/12/2016	8	31	-1	24/04/2017	10	38	72	4	58±13	19±6	-1±2	6±8	50±8
2017/2018	15/12/2017	25	23	-9	03/05/2018	0	28	55	6	48±15	24±6	-4±3	27±14	21±3
2018/2019	13/12/2018	15	19	-2	02/05/2019	1	20	55	6	51±17	21±7	-1±3	21±14	30±7
2019/2020	03/10/2019	-			12/05/2020	4	13	68	7	49±24	24±9	-1±3	32±20	20±5

142 The seasonal mean values of H_i , h_s , H_{gi} , and H_{ci} were calculated by the SIMBA algorithm (Cheng et al., 2020). The
 143 seasonal mean value of ice freeboard (H_{sfb}) was calculated based on time series of snow depth (h_s), granular ice thickness
 144 (H_{gi}) and columnar ice thickness (H_i) according to the Archimedes' principle: $H_{sfb} = H_i + H_{gi} - (h_s \rho_s + H_{gi} \rho_{gi} +$
 145 $H_i \rho_i) / \rho_w$, where ρ_s , ρ_{gi} , ρ_i and ρ_w are seasonal mean densities of snow, granular-ice and columnar ice and lake water,
 146 assumed to be 320 kg/m³, 890 kg/m³ and 910 kg/m³ and 1000 kg/m³, respectively. The STD is the standard deviation.

147

148 2.2.2 SIMBA buoy

149 SIMBA is a thermistor string-based Snow and Ice Mass Balance Apparatus. It has been developed
 150 by the Scottish Association for Marine Science (SAMS) Research Services Ltd (SRSL) in UK.
 151 SIMBA consists of a simple, robust thermistor string with 240 temperature sensors distributed evenly
 152 (2 cm intervals) along a 4.8 m long heat-shrink PVC plastic sleeve coated flat white wire. White heat-
 153 shrink sleeve is used to minimize the possibility of solar heating of the sensors. The accuracy of the
 154 SIMBA thermistor sensor is ± 0.01 °C, which is comparable with other type of thermistor string based
 155 IMBs (Jackson et al., 2013). Each sensor measures the environment temperature (SIMBA-ET). The
 156 resolution of the thermistor sensor is 0.0625°C, i.e., smaller changes cannot be detected even if the
 157 absolute accuracy of the sensor would allow it. In addition, the thermistor chain is equipped with
 158 heaters, i.e. resistor components mounted next to the temperature-sensing elements. A weak voltage
 159 (8 V) supply is connected to provide gentle identical heating of each sensor on the chain. After a short
 160 heating period, often 60 or 90 s, the heating temperatures (SIMBA-HT) are recorded. The SIMBA-
 161 HT reacts differently among the medium (air, snow, ice and water) which a sensor lies in. Therefore,
 162 the heating temperature profiles can greatly enhance the detection of the interfaces between air, snow,



163 ice and water. The heating cycle is applied once per day. The SIMBA-HT is controlled not to disturb
164 the SIMBA-ET measurements which are carried out typically 4 times per day (Jackson et al., 2013).
165 A SIMBA also includes a built-in GPS to record SIMBA drift positions (for sea ice applications), a
166 magnetometer for tilt and floe rotation, a barometer for surface air pressure, and an external sensor to
167 measure near-surface ambient air temperature. An iridium modem is applied for data transmission.
168 SIMBA has been used in various field campaigns targeting snow and ice mass balance in seasonally
169 ice-covers in lakes (Cheng et al., 2014) and Polar Oceans (Hoppmann et al. 2015; Provost et al. 2017;
170 Lei et al. 2018, 2021). Table 1 presents a summary of SIMBA observations in Lake Orajärvi.

171

172 **2.3 Weather station**

173 Meteorological data were collected at FMI-ARC station (67.3666°N, 26.6290°E, WMO code 02836)
174 11 km from Lake Orajärvi. The data sets include wind speed (Va), air temperature (Ta), relative
175 humidity (RH), cloudiness (cn), longwave (Ql) and shortwave (Qs) radiation, snow depth on land (Hs)
176 and precipitation ($Prec$) (Table 2). The radiative fluxes were measured on a 10-m high tower above
177 treetops using Kipp&Zonen CM11 pyranometers (305-2800 nm) and Kipp&Zonen CG4
178 pyrgeometers (4500 - 42000 nm). Snow depth (Campbell Scientific SR50) and precipitation (OTT
179 Pluvio2) at ground level were also measured. All measurements were taken once a minute and
180 aggregated to 1-hour time intervals.

181

182 **3 Data description**

183 **3.1 SIMBA data**

184 The main output of a SIMBA buoy is the time series of environment (SIMBA-ET) and heating
185 (SIMBA-HT) temperature measured at different depths from the lake water through ice and snow to
186 air.

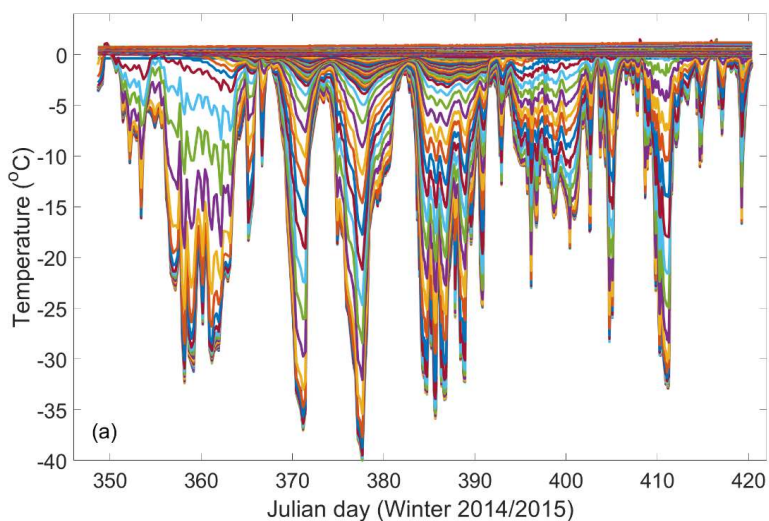
187

188 *3.1.1 SIMBA-ET*

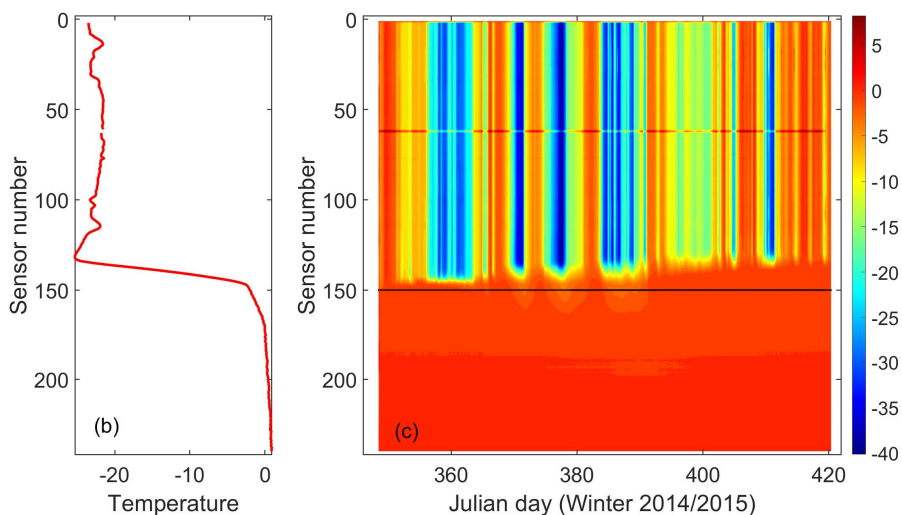
189 For each season, we have up to 241 time series of temperature (SIMBA-ET) at different depths. For
190 those sensors located in the air, the temperature differences between the sensors are small, as the air
191 in the lowermost 1.5 m layer mixes effectively and the sensors are close to each other. The
192 temperatures inside snow reveal much larger vertical gradients because snow has a small thermal heat



193 conductivity. The temperature profile in ice has smaller vertical gradient compared to that in snow,
194 since the thermal heat conductivity of ice is larger than that of snow. At the ice bottom, temperature
195 is at the freezing point and gradually increases towards the lake bottom. Figure 8 shows an example
196 of seasonal SIMBA-ET. One can estimate the heat fluxes within snow and ice, and those at the air-
197 snow, snow-ice, and ice-water interfaces.



198



199

200 Figure 3. Illustrations of SIMBA-ET data: a) Time series of SIMBA-ET during observation period;

201 b) One snapshot (19 Jan 2014 08:00 UTC) of vertical SIMBA-ET profile through air-snow-lake ice-

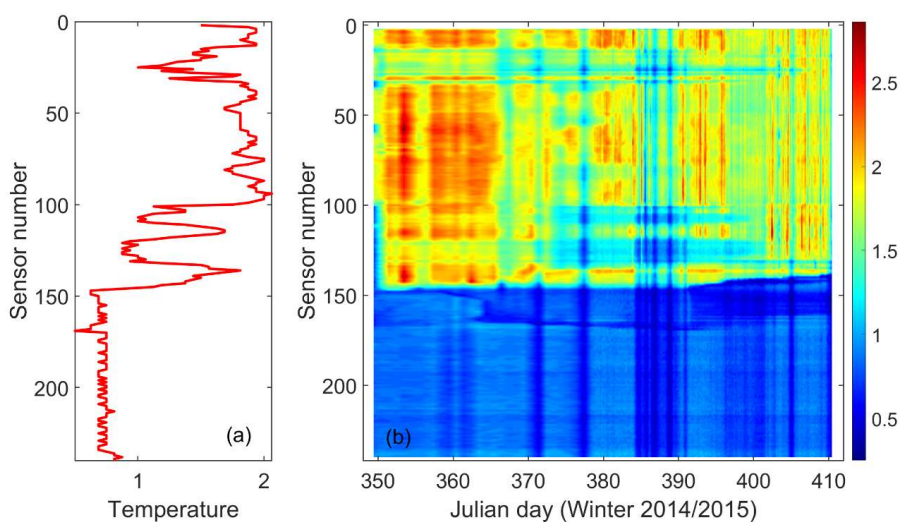


202 water; c) SIMBA-ET field observed by 240 sensors. Sensor 1 was placed in air and sensor 240 in
203 water.

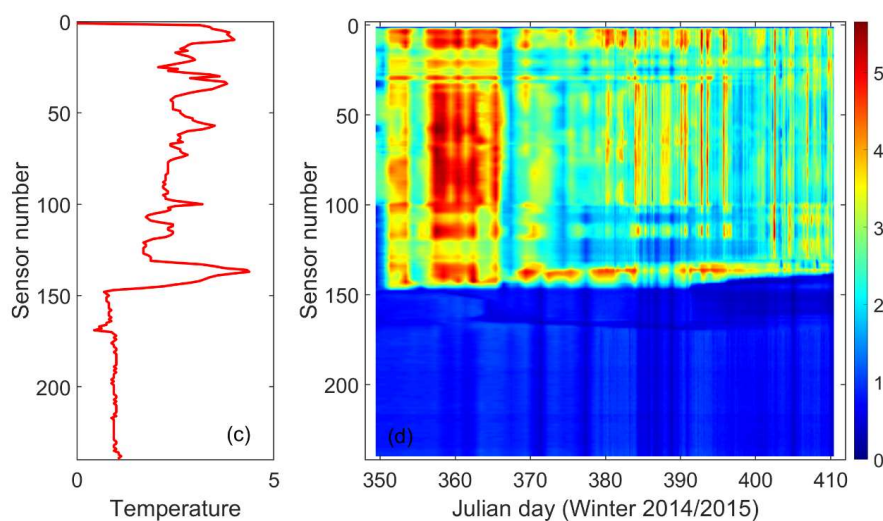
204

205 3.1.2 SIMBA-HT

206 SIMBA-HT shows the temperature increase in the medium each sensor was contacted during a short
207 heating period of 60 s and 90 s. The temperature changes are largely dependent on the thermal
208 diffusivity of the surrounding medium. Low heating power ensures that the temperature increasing
209 will not be too high to melt snow and ice in contact with the sensor and guarantee a fast restore of
210 environment temperature around the sensor before the next SIMBA-ET observation, and above all to
211 minimize SIMBA power consumption. One example of SIMBA-HT is given in Figure 9.



212



213

214 Figure 4. Illustrations of SIMBA-HT: a) a snapshot (25 January, 2015, 18:00 UTC) of vertical profile
215 of observed temperature increase after 60 s., b) SIMBA-HT (60s) field observed by 240 sensors; c)
216 Same as a) but after heating for 90 s., and d) SIMBA-HT (90s) field observed by 240 sensors;

217

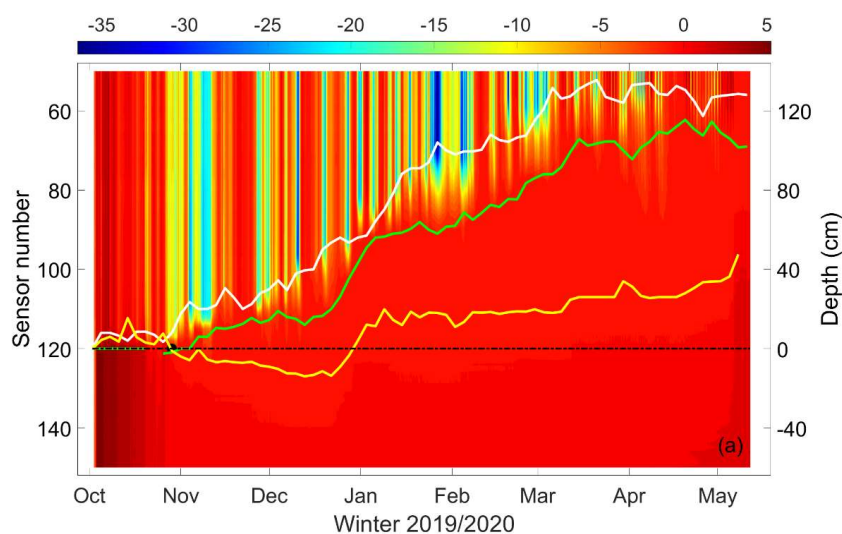
218 3.1.3 SIMBA snow depth and ice thickness

219 Snow depth and ice thickness are derived from SIMBA-ET and SIMBA-HT data. A common
220 procedure is to look SIMBA-ET temperature profiles manually and identify sudden changes of
221 vertical temperature gradient to locate the air-snow, snow-ice and ice-water interfaces. The snow
222 depth is then calculated as the distance between the air-snow and snow-ice interfaces, and the ice
223 thickness is the distance between the snow-ice and ice-water interfaces. However, a manual procedure
224 is a heavy task, especially if SIMBA operation covers long period or one would need real time SIMBA
225 results. Several studies have been carried out aiming development of an algorithm to obtain snow
226 depth and ice thickness automatically (Liao et al., 2019, Zuo, et al., 2019, Cheng et al., 2020).

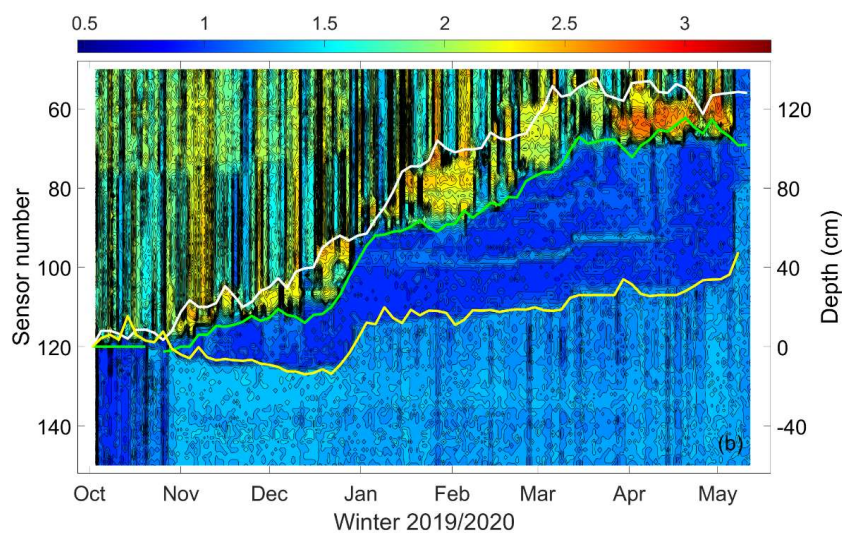
227 Below we present an example of the application of the Cheng et al, (2020) algorithm to retrieve snow
228 depth and ice thickness from SIMBA data observed in Lake Orajärvi. When SIMBA was deployed,
229 the initial sensor position at snow-ice interface is known and we defined it as Z_{gi0} , i.e. zero reference
230 position for granular ice. During observation period, in case if initial snow-ice interface is moving
231 upward from Z_{gi0} , which is a common phenomenon in Arctic lakes, the distance between Z_{gi0} and
232 moving snow-ice interface is the new granular ice thickness formed by snow to ice transformation.



233 The depth difference between total ice thickness and granular ice thickness is the congelation ice
234 formed at the ice bottom. Figure 5 shows the air-snow, snow-ice and ice-water interfaces with
235 SIMBA-ET (a) and SIMBA-HT (b) as the background. For better clarity, 5-day running average can
236 be produced as the final products.
237



238



239

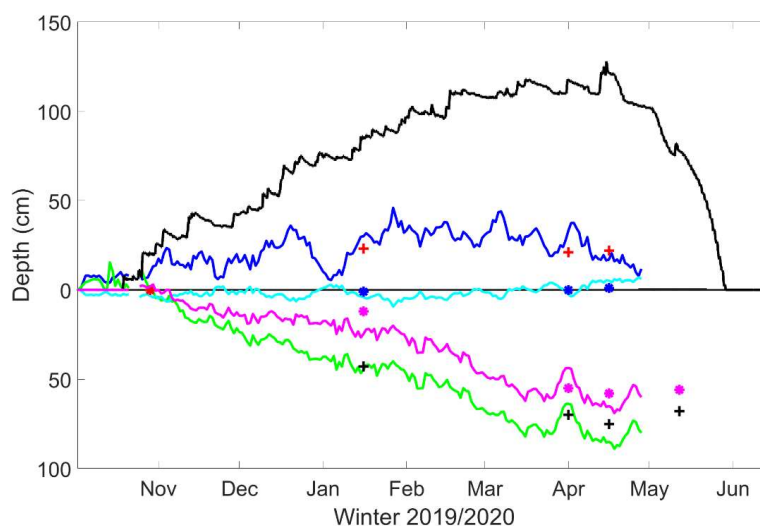
240 Figure 5. Time series of sensor position for the air-snow (white), snow-ice (green) and ice-water
241 (yellow) interfaces, identified applying the SIMBA algorithm. The SIMBA-ET observation is



242 illustrated as background in a), and SIMBA-HT ratio (HT60/HT90) in b). The black dash line shows
243 the sensor number (120) at the initial ice surface (Z_{gio}). For clarity, we only illustrate sensors 50 –
244 150.

245

246 Using snow/ice interface as the zero-reference level, time series can be calculated for the snow depth,
247 snow-ice thickness, total ice thicknesses, and ice freeboard (Fig. 6). Figure 6 is an example of the
248 2019/2020 time series, indicating that the lake ice was mainly granular ice, which was related to
249 heavy snow fall during the ice season (the snow depth observed at FMI-ARC weather station on land
250 was highest in a decade).



251

252 Figure 6. Products derived on the basis of SIMBA data: snow depth (blue), ice freeboard (cyan),
253 granular ice thickness (magenta), and total ice thickness (green). The symbols represent manual
254 observations of snow depth (+), ice freeboard (•), granular ice thickness (•) and total ice thickness
255 (+). The black solid line denotes the snow depth on land.

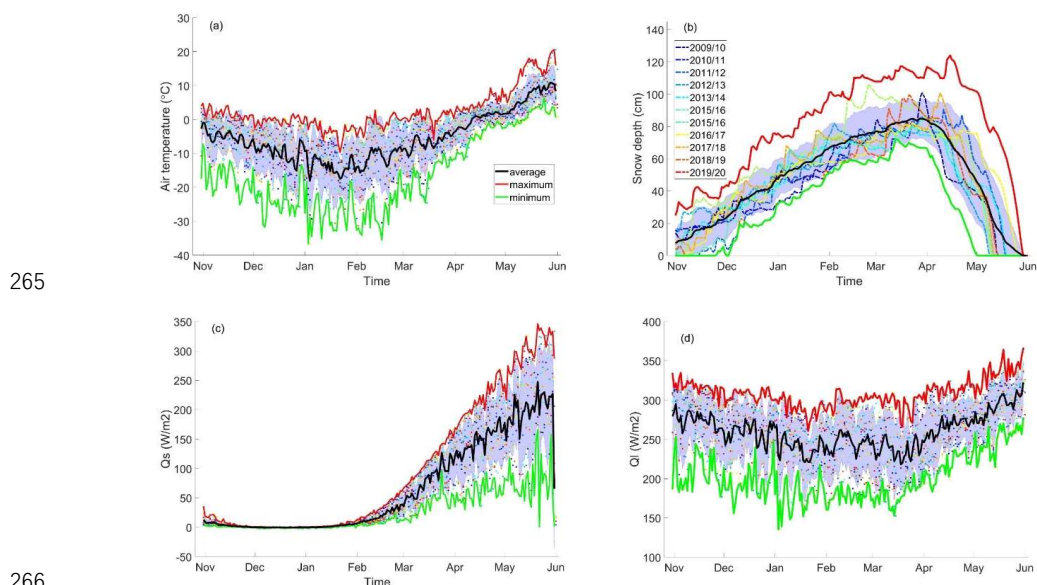
256

257 3.2 Weather data

258 The observed daily mean values of meteorological parameters for all seasons are presented in Figure
259 7. The inter-annual mean, maximum and minimum air temperatures are -2.5 °C, -16.5 °C and -5.5 °C,
260 respectively. The air temperature reveals a constant decreasing pattern from November to January.
261 The coldest months are January and February. From March onward, the air temperature increased



262 gradually due to increasing solar radiation (Fig. 7c). The inter-annual average, maximum and
 263 minimum downward longwave radiative fluxes are 259 W/m^2 , 309 W/m^2 , and 201 W/m^2 , respectively.
 264 The corresponding values for downward shortwave radiative fluxes are 64 W/m^2 , 97 W/m^2 , 26 W/m^2 .



266
 267 Figure 7. The observed (dots) daily mean air temperature (a), snow depth (b), downward shortwave
 268 (c), and longwave (d) radiative fluxes for each ice season between 1 November and 31 May. The solid
 269 lines represent decadal daily maximum (red), minimum (green) and average (black) values. The
 270 shadow area represents the standard deviation (STD). For snow depth, daily mean values are given
 271 as thin color lines.

272
 273 Table 2 Summary of various meteorological and physical observations between 1 November and 31
 274 May. For meteorological parameters (V_a , T_a , RH , cn , Q_s , Q_l) the values are seasonal mean \pm standard
 275 deviation.

Season	V_a <i>m/s</i>	T_a <i>°C</i>	RH <i>(%)</i>	cn <i>(-)</i>	Q_s <i>W/m²</i>	Q_l <i>W/m²</i>	T_{prec} <i>(mm)</i>	H_{smax} <i>(cm)</i>	FDD <i>°C</i>	TDD <i>°C</i>
2009/2010	2.2±0.3	-6.8±9.4	84±9	0.7±0.1	62.9±76.8	267±31	201	101	-1717	304
2010/2011	2.2±0.6	-8±9.5	83±9	0.6±0.1	64.1±76.5	259±27	157	72	-1955	286
2011/2012	2.4±0.4	-5.1±7.2	84±11	0.7±0.1	64.4±82.3	264±21	272	91	-1308	239
2012/2013	2.2±0.2	-6.3±8.5	80±13	0.6±0.2	67±85.6	250±31	192	82	-1683	346



2013/2014	2.6±0.4	-4.6±6.4	81±10	0.7±0.1	61.6±81.8	261±19	267	81	-1214	243
2014/2015	2.7±0.6	-4.3±6.6	84±8	0.7±0.1	55.8±67.2	264±21	286	87	-1148	249
2015/2016	2.3±0.3	-4.2±8.4	84±10	0.7±0.1	61.5±81	265±25	287	106	-1261	354
2016/2017	2.8±0.3	-5.9±4.7	81±10	0.7±0.1	64.9±81.2	252±14	186	82	-1338	101
2017/2018	2.5±0.4	-6±8.7	80±12	0.7±0.2	66.5±82.7	256±27	219	101	-1615	362
2018/2019	2.7±0.4	-5.4±7.9	84±10	0.6±0.1	63.5±79.8	258±26	256	100	-1432	293
2019/2020	2.8±0.5	-5±5.1	84±13	0.6±0.1	70.1±92.9	258±13	285	124	-1242	188

276 *Tprec*: total accumulated precipitation in water equivalent (mm); Hsmax: the maximum observed snow depth on land.

277 FDD: The accumulated freezing degree day: the sum of daily mean air temperature below freezing point; TDD: The

278 accumulated thawing degree day: the sum of daily mean air temperature above freezing point.

279

280 Figure 7b clearly indicates that snow depth for the 2019/2020 season represented an extreme

281 condition in a decade. There is an increasing trend of total precipitation during the ice season (Fig.

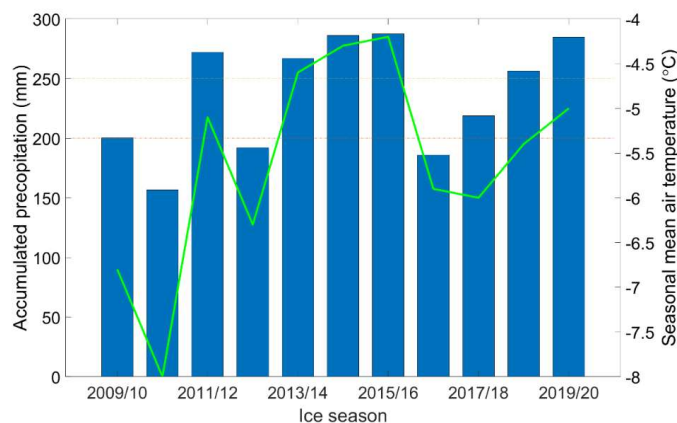
282 8). The total seasonal accumulated total precipitation is highly correlated (correlation coefficient $r =$

283 0.93) with the seasonal mean air temperature. The correlations between seasonal mean/maximum

284 snow depth and corresponding air temperature are much lower $r = 0.40$ and $r = 0.38$, respectively.

285 The correlation between total accumulated precipitation and maximum snow depth was 0.55. The

286 difference is contributed by the snow drift and changes of snow metamorphism.



287

288 Figure 8. The accumulated total precipitation and mean air temperature between 1 November and 31
 289 May.

290

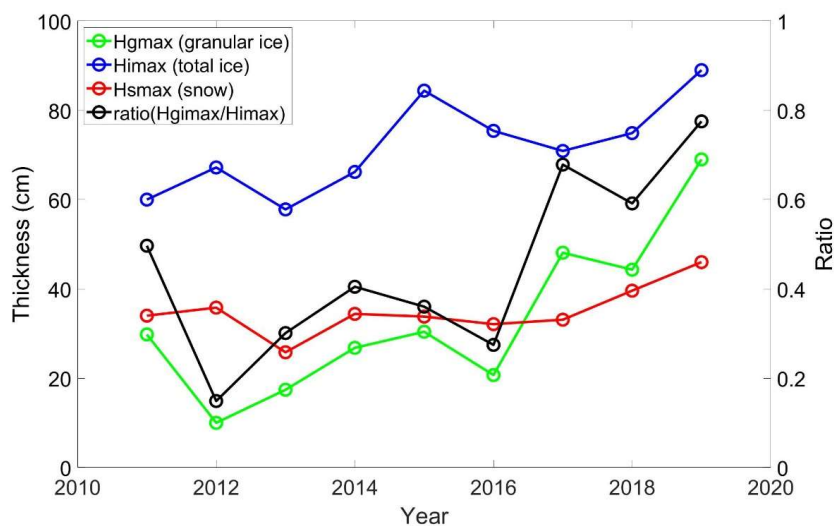


291

292 4. Discussions

293 4.1 Inter-annual variation of SIMBA snow and ice products

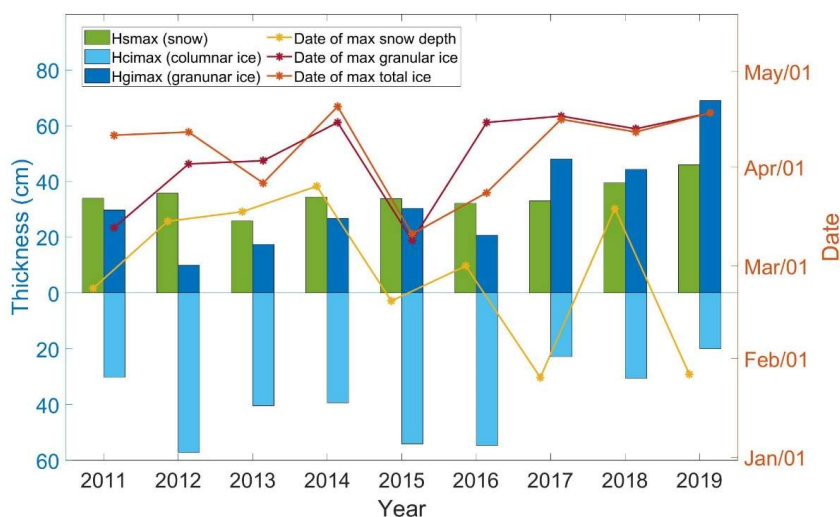
294 Applying the SIMBA algorithm (Cheng et al., 2020), we obtained lake snow and ice products for all
295 seasons (see data availability). Figure 9 shows the observed seasonal maximum values for the snow
296 depth, maximum total ice thickness, and maximum granular ice thickness. During the observation
297 period, both snow depth and ice thickness showed increasing trends. The increase of granular ice
298 thickness is the fastest among all the snow and ice components. It reached the maximum 80% of the
299 total ice thickness in 2019/2020. In Lake Orajärvi, snow mass has contributed to the ice thickness
300 during every winter season. The maximum granular ice thickness was on average about 40% of the
301 maximum total ice thickness during the data period. For all seasons, the correlation coefficient
302 between the maximum granular ice thickness and the maximum ice thickness was 0.64. The
303 occurrence of maximum lake snow is, on the average, about one month prior to the maximum granular
304 ice formation (Fig. 10). Because of snow to ice transformation, the time series of snow depth in the
305 lake is not correlated with the snow depth on land. The snow depth on lake ice ranged from 25 to 43%
306 of that on land. On the average the ratio was 0.33, some 11% less than observed for a lake in southern
307 Finland (Kärkäs, 2000). In several seasons, when SIMBA were recovered in late April or early May,
308 the entire snow layer on lake ice was transferred to granular ice. Granular ice reached its maximum
309 value when the ice surface was free of snow.



310



311 Figure 9. SIMBA observed seasonal maximum snow depth (red), maximum total ice thickness (blue),
312 maximum granular ice thickness (green) and the ratio between granular ice and total ice thickness
313 (black) during observation seasons.



314
315 Figure 10. Seasonal maximum snow depth, granular ice thicknesses, congelation ice thicknesses,
316 and the date when those values were observed.

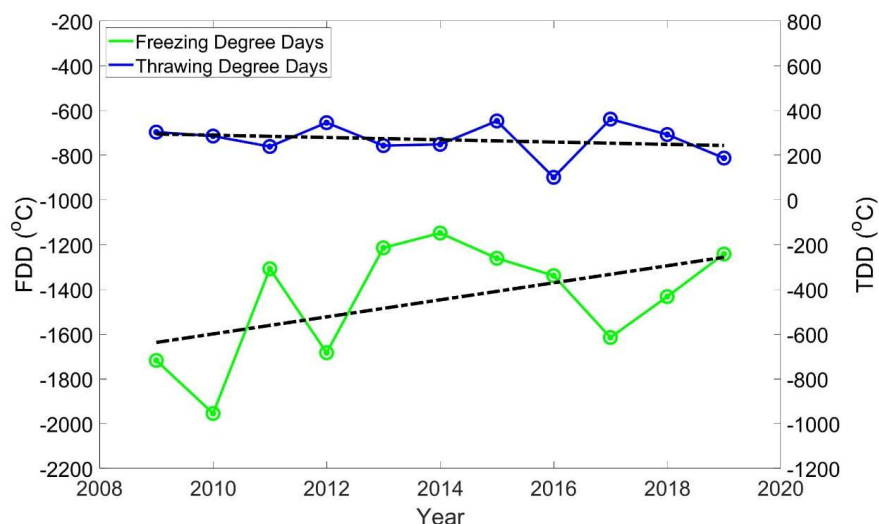
318 4.2 Inter-annual variation of temperature conditions

319 According to weather observations in Sodankylä, the air temperature increased by about 0.16 °C/year
320 during the last decade. For the period from 1980 – 2020, the air temperature has an increasing trend
321 of about 0.06 °C/year. On the average, the increase of air temperature in last decade is about 3 times
322 faster than the past 40 years in agreement with the findings of Przybylak and Wszyński (2020) for
323 the high Arctic. The accumulated precipitation correlated better to the maximum snow depth on land
324 ($r = 0.55$) than the mean snow depth ($r = 0.45$). It is, however, not correlated ($r = 0.21$) with snow
325 depth on the lake ice.

326 The seasonal integrated FDD and TDD for each winter season are shown in Figure 11. A negative
327 decreasing of FDD was seen in response to the increase of air temperature. FDD is directly linked
328 with thermodynamic ice formation. During a given period, a decrease of FDD is expected to result in
329 less formation of columnar ice. However, during our observation period, the total ice thickness
330 revealed an increasing trend. The increase of ice thickness is due to snow-ice formation. The trend of



331 TDD is very insignificant, suggesting that the melting of lake ice due to temperature increase has not
332 increased much during the observation decade.



333

334 Figure 11. The seasonal accumulated freezing degree day (FDD) and thaw degree day (TDD)
335 during the observation period (2009/2010 – 2019/2020).

336

337 4.3 Challenges of the SIMBA program

338 SIMBA observations in Lake Orajärvi represent a small but sustainable program, so far ran for a
339 decade. A few times we have encountered malfunction of SIMBA, especially in the early phases of
340 the SIMBA program. In recent years, SIMBA has become more robust without need for heavy-duty
341 maintenances during field measurements, and the system has been remarkably improved with respect
342 to the quality of HT measurements. Several snow and ice products can be derived from SIMBA's two
343 type of temperature (SIMBA-ET and SIMBA-HT) measurements. The SIMBA program has largely
344 benefited from the Sodankylä supersite infrastructure, where the comprehensive and high standard
345 meteorological observations are available.

346 Challenges remain in further improvement of the SIMBA program. Due to safety issues, SIMBA must
347 be deployed and recovered when ice is strong enough. Hence, the early freeze-up and late break-up
348 cannot be monitored. In Autumn 2019, a wooden floating raft was deployed and anchored in Lake
349 Orajärvi. SIMBA was, for the first time, deployed during ice-free season on 1 October. This kind of
350 deployment will be carried out also in the future, allowing year-round SIMBA measurements.



351 Part of the thermistor chain exposed in the air above the snow surface may suffer from frost in winter
352 or from solar heating in spring, and also the sensors in the upper layers of snow and ice may suffer
353 from solar heating, resulting in large uncertainties in SIMBA-ET and SIMBA-HT readings. To
354 compensate the effect of temperature errors on snow depth detection, one solution is to deploy
355 Acoustic Rangefinder Sounders (ARS) to measure the evolution of snow surface. In fact, an ARS has
356 been deployed in the past two winter seasons. These data sets can also be used to understand the effect
357 of wind on snow drift and quantify snow surface sublimation in winter.

358 During the melting season, both SIMBA-ET and SIMBA-HT strongly raise in the upper part of the
359 ice resulting an isothermal status of the entire ice column. In this condition, SIMBA snow depth and
360 ice thickness values are liable to large errors. Combination of SIMBA observations and numerical
361 model experiments may yield more reliable results in such conditions.

362 SIMBA measurements have been taken automatically, but it is still important to carry out manual on
363 site observations, such as collecting ice core and snow samples, as such observations cannot be made
364 by automatic instruments.

365

366 **4 Data availability**

367 The data are archived at <https://zenodo.org/record/4559368#.YEIYOtyxVPZ> (Cheng et al., 2021).

368 The 4 zip-files should be unzipped in different file folders preferably using zip-file names as the
369 folder names. A readme file exists in each folder. The manual in situ snow depth and ice thickness
370 observation for 2009/2010 - 2012/2013 as well as a description of SIMBA deployment and recovery
371 for each ice season (SIMBA_D&R_all_Years.docx) are provided.

372

373 **5 Conclusions**

374 A thermistor string-based snow and ice mass balance apparatus (SIMBA) has been deployed in an
375 Arctic lake since 2009. The measurements covered most part of the ice season from mid-December
376 to late April/early May. SIMBA-ET and SIMBA-HT temperature observations are described in this
377 paper. The daily snow depth and ice thickness were derived from SIMBA temperature field applying
378 a validated automatic algorithm (Cheng et al., 2020). The meteorological parameters for winter
379 seasons (1 November - 31 May) are also collected and discussed. During the investigation decade,
380 the air temperature in the ice season has had an increasing trend of 0.16 °C/year. The warming rate is



381 comparable to the result find for the high Arctic by Przybylak and Wyszyński (2020). The increase of
382 air temperature in winter season is highly correlated (0.93) with seasonal total accumulated
383 precipitation. The precipitation in season 2019/2020 represented an extreme episode during the study
384 decade. Despite of the air temperature increase, the total maximum ice thickness in the lake has an
385 increasing trend. The increase of maximum ice thickness is due to the increase of granular ice. The
386 interannual variability of maximum granular ice thickness is large ranging from 15 to 80% of the total
387 maximum ice thickness. The time series of the SIMBA ET and HT allow identification of moving
388 air-snow, snow-ice and ice-water interfaces. Because of the air temperature increase, the seasonal
389 accumulated FDD is reducing, suggesting reduced formation of columnar ice and, hence, a smaller
390 role of air temperature in controlling the ice thickness. On the contrary, the role of precipitation on
391 total ice formation is enhanced. The trend in TDD was negligible, suggesting that the effect of air
392 temperature on ice melting has remained unchanged.

393 To our knowledge, this is the first decadal-scale SIMBA data set ever collected from an Arctic lake.
394 The data provides information on snow and ice mass balance and the controlling atmospheric factors.
395 The measurements will continue in the future.

396 The weather observations, e.g. decadal time series of daily maximum and minimum weather
397 parameters, can be used to estimate snow and ice conditions in the lake applying a snow/ice model
398 (e.g. Cheng et al., 2014). The SIMBA data are not only suitable for snow/ice surface heat and mass
399 balance studies. The temperatures at the ice bottom and in the water below are valuable to understand
400 the lake thermal structure and water-ice heat transfer (Huang et al., 2019b).

401 The SIMBA program, with Lake Orajärvi as a testbed, offers excellent opportunities for
402 dissemination of cryospheric knowledge and related outreach, providing rich possibilities for
403 community collaborations both nationally and internationally. The observed changes in snow depth
404 and composition of lake ice contribute to better understanding of cryospheric aspects of climate
405 change. For example, parameterizations of the discovered snow and ice processes can be improved
406 in climate models.

407 Snow and ice measurements similar to those in Lake Orajärvi have been recently initiated in
408 Wulaingsuhai lake in an arid climate zone in Inner-Mongolia of China. The observations focused on
409 lake ice mass balance (Lu et al., 2020) and energy budget, in particular the solar radiation (Cao et al.,
410 2020). In a long run, the corresponding lake snow and ice measurements at both sites and possible



411 similar observations in a thermokarst lake (e.g. Huang et al, 2019a, 2019b) at Qinghai-Tibet Plateau,
412 often referred to as the “Third Pole of the Earth” can be used together to carry out coordinated research.

413

414 **Acknowledgement**

415 We are grateful to Mr. Pekka Kosloff for carrying out fieldwork in Lake Orajärvi for all the winter
416 seasons. The logistical assistance provided by Mr. Jyrki Mattanen in FMI-ARC, Sodankylä are
417 acknowledged. The study was for financial support by FMI long-term sustainable SIMBA program.
418 The data analyses were partly supported by the European Union’s Horizon 2020 research and
419 innovation programme [727890 – INTAROS]; Academy of Finland under contract 317999, and the
420 National Key Research and Development Program of China (No. 2017YFE0111700 – MARIS)

421

422

423 **References**

424 Anderson, E.J., Fujisaki-Manome, A., Kessler, J., Lang, G.A., Chu, P. Y., Kelley, J.G.W., Chen, Y.,
425 and Wang, J.: Ice Forecasting in the Next-Generation Great Lakes Operational Forecast System
426 (GLOFS), *J. Mar. Sci. Eng.*, 6, 123; doi:10.3390/jmse6040123, 2018.

427 Ballinger, T.J., Overland, J.W., Wang, M., Bhatt, U.S., Hanna, E., Hanssen-Bauer, I., Kim, S.-J.,
428 Thoman, R.L., and Walsh, J.E.: Surface air temperature, Arctic Report Card, [DOI: 10.25923/gcw8-
429 2z06](https://doi.org/10.25923/gcw8-2z06), 2020.

430 Bintanja, R.: The impact of Arctic warming on increased rainfall, *Scientific Report*.
431 DOI:10.1038/s41598-018-34450-3, 2018.

432 Box, J.E. and 19 others: Key indicators of Arctic climate change: 1971–2017, *Environ. Res. Lett.* 14
433 045010, 2019.

434 Brown, L. C. and Duguay, C.R.: The response and role of ice cover in lake climate interactions.
435 *Progress in Physical Geography: Earth and Environment* 34(5), 671–704, 2010.

436 Cheng, B., Vihma T., Rontu, L., Kontu, A. Kheyrollah Pour H., Duguay C. and Pulliainen, J.:
437 Evolution of snow and ice temperature, thickness and energy balance in Lake Orajärvi, northern
438 Finland, *Tellus A: Dynamic Meteorology and Oceanography* 66(1), 21564, 2014.

439 Cheng, Y., Cheng, B., Zheng, F., Vihma, T., Kontu, A., Yang, Q. and Liao, Z.: Air/snow, snow/ice and
440 ice/water interfaces detection from high-resolution vertical temperature profiles measured by ice



- 441 mass-balance buoys on an Arctic lake, *Annals of Glaciology* 1–11. <https://doi.org/10.1017/>
442 [aog.2020.51](https://doi.org/10.1017/aog.2020.51), 2020
- 443 Cheng, B., Cheng, Y., Vihma, T., Kontu, A., Zheng, F., Lemmetyinen, J., and Pulliainen, J.: SIMBA
444 snow/ice mass balance buoy data and weather station data [Data set]. *Earth System Science Data*
445 (ESSD). Zenodo. <http://doi.org/10.5281/zenodo.4559368>, 2021.
- 446 Cao, X., Lu, P., Leppäranta, M., Arvola, L., Huotari, J., Shi, X., Li, G., and Li, Z.: Solar radiation
447 transfer for an ice-covered lake in the central Asian arid climate zone. *Inland Waters*,
448 doi:10.1080/20442041.2020.1790274, 2020.
- 449 Filazzola, A., Brown, C., Dettlaff, M.A., Batbaatar, A., Grenke, J., Bao, T., Heida, I.P., and Cahill
450 Jr, J.F.: The effects of livestock grazing on biodiversity are multitrophic: a meta-analysis, *Ecology*
451 *Letters*, 23: 1298–1309, <https://publons.com/publon/10.1111/ele.13527>, 2020.
- 452 Hoppmann, M., Nicolaus, M., Hunkeler, P. A., Heil, H., Behrens, L.-K., König-Langlo, G., and Gerdes,
453 R.: Seasonal evolution of an ice-shelf influenced fast-ice regime, derived from an autonomous
454 thermistor chain, *J. Geophys. Res. Oceans*, 120, 1703–1724, doi:10.1002/2014JC010327, 2015.
- 455 Huang, W., Cheng, B., Zhang, J., Zhang, Z., Vihma, T., Li, Z., and Niu, F.: Modeling experiments on
456 seasonal lake ice mass and energy balance in the Qinghai–Tibet Plateau: a case study, *Hydrol. Earth*
457 *Syst. Sci.*, 23, 2173–2186, <https://doi.org/10.5194/hess-23-2173-2019>, 2019a.
- 458 Huang, W., Zhang, J., Leppäranta, M., Li, Z., Cheng, B. and Lin, Z.: Thermal structure and water-ice
459 heat transfer in a shallow ice-covered thermokarst lake in central Qinghai-Tibet Plateau. *Journal of*
460 *Hydrology*, 578, [124122]. <https://doi.org/10.1016/j.jhydrol.2019.124122>, 2019b
- 461 Jackson, K., Wilkinson, J., Maksym, T., Meldrum, D., Beckers, J., Haas, C., and Mackenzie, D.: A
462 novel and low-cost sea ice mass balance 1010 buoy. *J. Atmos. Ocean. Tech.* 30(11), 2676–2688. DOI:
463 10.1175/JTECH-D-13-00058.1., 2013
- 464 Kang, K.-K., Duguay, C.R., Lemmetyinen, J., and Gel, Y.: Estimation of ice thickness on large
465 northern lakes from AMSR-E brightness temperature measurements. *Remote Sensing of*
466 *Environment* 150, 1–19, doi: 10.1016/j.rse.2014.04.016, 2014.
- 467 Kärkäs, E.: The ice season of Lake Pääjärvi in southern Finland. *Geophysical Research Letters* 36(1–
468 2), 85–94, 2000.
- 469 Lei, R., Cheng, B., Heil, P., Vihma, T., Wang, J., Ji, Q., and Zhang, Z.: Seasonal and interannual
470 variations of sea ice mass balance from the central Arctic to the Greenland Sea. *Journal of*



- 471 Geophysical Research: Oceans 123(4), 2422–2439, 2018.
- 472 Lei, R., Hoppmann, M., Cheng, B., Zuo, G., Gui, D., Cai, Q., Belter, H. J., and Yang, W.: Seasonal
473 changes in sea ice kinematics and deformation in the Pacific sector of the Arctic Ocean in 2018/19,
474 The Cryosphere, 15, 1321–1341, <https://doi.org/10.5194/tc-15-1321-2021>, 2021.
- 475 Leppäranta, M.: Modelling the formation and decay of lake ice. In George G (ed.), The Impact of
476 Climate Change on European Lakes. Dordrecht, Netherlands: Springer, pp. 63–83, 2010.
- 477 Leppäranta, M.: Freezing of Lakes and the Evolution of Their Ice Cover. Berlin Heidelberg: Springer,
478 2015.
- 479 Liao, Z., Cheng, B., Zhao, J., Vihma, T., Jackson, K., Yang, Q., Yang, Y., Zhang, L., Li, Z. Qiu, Y. and
480 Cheng, X.: Snow depth and ice thickness derived from SIMBA ice mass balance buoy data using an
481 automated algorithm. International Journal of Digital Earth 12(8), 962–979, 2019.
- 482 Lu, P., Cao, X., Li, G., Huang, W., Leppäranta, M., Arvola, L., Huotari, J., and Li, Z.: Mass and heat
483 balance of a lake ice cover in the central Asian arid climate zone. Water, 12(10), 2888,
484 doi:10.3390/w12102888, 2020.
- 485 Mermoz, S., Allain-Bailhache, S., Bernier, M., Pottier, E., Sanden, J. J. Van Der, and Chokman. K.:
486 Retrieval of river ice thickness from C-band PolSAR data. IEEE Transactions on Geoscience and
487 Remote Sensing 99, 1–11, doi: 10.1109/TGRS.2013.2269014, 2013.
- 488 Provost, C., Sennechaël, N., Miguet, J., Itkin, P., Rosel, A., Koenig, Z., Villaceros-Robineau, N., and
489 Granskog, M.A.: Observations of flooding and snow-ice formation in a thinner Arctic sea-ice regime
490 during the N-ICE2015 campaign: influence of basal ice melt and storms. Journal of Geophysical
491 Research: Oceans 122(9), 7115–7134, doi:10.1002/2016JC012011, 2017.
- 492 Przybylak R, Wszyński P.: Air temperature changes in the Arctic in the period 1951– 2015 in the
493 light of observational and reanalysis data. Theor. Appl. Climatol. 139: (1–2):75–94.
494 DOI: 10.1007/s00704-019-02952-3, 2020
- 495 Sharma, S., Blagrove, K., Magnuson, J.J., M. O’Reilly, C., Oliver, S., D. Batt, R., R. Magee, M.,
496 Straile, D., Weyhenmeyer, G.A. Winslow, L., Woolway, R.I.: Widespread loss of lake ice around the
497 Northern Hemisphere in a warming world. Nat. Clim. Chang. 9, 227–231.
498 <https://doi.org/10.1038/s41558-018-0393-5>, 2019.
- 499 Tikkanen, M.: Climate. In: The Physical Geography of Fennoscandia (ed. M. Seppälä). Oxford:
500 Oxford University Press, pp. 96112, 2005.



501 Wei L., Deng X., Cheng B., Vihma T., Hannula H., Qin T., and Pulliainen J.: The impact of
502 meteorological conditions on snow and ice thickness in an Arctic lake. *Tellus - Series A: Dynamic*
503 *Meteorology and Oceanography*, Vol 68: 1~12, 2016.

504 Woolway, R., Weyhenmeyer, G.A., Schmid, Dokulil, M.T., de Eyto, E., Maberly, S.C., May, L., and
505 Merchant, C. J.: Substantial increase in minimum lake surface temperatures under climate change.
506 *Climatic Change* 155, 81–94. <https://doi.org/10.1007/s10584-019-02465-y>, 2019.

507 Wu, Y., Duguay, C, R, and Xu, L.: Assessment of machine learning classifiers for global lake ice
508 cover mapping from MODIS TOA reflectance data, *Remote Sensing of Environment*, Vol 253,
509 112206 <https://doi.org/10.1016/j.rse.2020.112206>, 2021.

510 Zuo, G., Dou, Y., Lei, R.: Discrimination algorithm and procedure of snow depth and sea ice thickness
511 determination using measurements of the vertical ice temperature profile by the ice-tethered buoys.
512 *Sensors* 18, 4162. <https://doi.org/10.3390/s1812416>, 2018.

513
514
515